Antenna sensor skin for fatigue crack detection and monitoring

Srikar Deshmukh, Xiang Xu, Irshad Mohammad and Haiying Huang*

Department of Mechanical and Aerospace Engineering, University of Texas at Arlington, USA

Abstract. This paper presents a flexible low-profile antenna sensor for fatigue crack detection and monitoring. The sensor was inspired by the sense of pain in bio-systems as a protection mechanism. Because the antenna sensor does not need wiring for power supply or data transmission, it is an ideal candidate as sensing elements for the implementation of engineering sensor skins with a dense sensor distribution. Based on the principle of microstrip patch antenna, the antenna sensor is essentially an electromagnetic cavity that radiates at certain resonant frequencies. By implementing a metallic structure as the ground plane of the antenna sensor, crack development in the metallic structure due to fatigue loading can be detected from the resonant frequency shift of the antenna sensor. A monostatic microwave radar system was developed to interrogate the antenna sensor remotely. Fabrication and characterization of the antenna sensor for crack monitoring as well as the implementation of the remote interrogation system are presented.

Keywords: sensor skin; antenna sensor; wireless sensor; passive sensor; sensor; microwave radar.

1. Introduction

The sense of pain is an important self-protecting mechanism for many bio-systems. The "pain" sensors, i.e., nociceptors, are sensory neurons specialized to detect intense stimuli that causes or could potentially cause tissue damages (Woolf and Ma 2007, Smith 1989). Sensing these stimuli enables bio-systems to take necessary actions such as rapid withdrawal to remove the body from the noxious stimuli and thus prevents future tissue damages. Therefore, nociceptors are the first line of defense for the bio-systems to maintain the body's integrity. People who are not sensitive to pain due to the lack of nociceptors can experience severe tissues injuries such as burn and self-mutilation because the hostile stimuli that cause tissue damages are not promptly detected (Axelrod and Hilz 2003, Verpoorten *et al.* 2006). This is analogous to man-made mechanical systems that do not have embedded sensors that can provide information about the development of structural damages such as fatigue cracks, corrosions, debonding, *etc*. One goal of Structural Health Monitoring (SHM) is to enable engineering systems to detect these damages autonomously (Giurgiutiu and Bao 2002, Chang and Ihn 2004), and thus equip them with the sensation of pain. Unlike the biological skins that have a large number of sensors densely distributed over a large area, most current SHM systems can only implement a few sensors at strategic locations. As a result, the sensitivity and spatial resolution of existing SHM systems are much inferior to those of bio-skins. Several researchers have attempted to

---

*Corresponding Author, Assistant Professor, E-mail: huang@uta.edu

develop engineered sensing skin for SHM purpose (Carlson *et al.* 2006, Zhang *et al.* 2006, Jang *et al.* 2006, Loh *et al.* 2009, Shoureshi and Shen 2006). The major challenge in sensing skin development is the wiring needed for power supply and signal transmission. Meandering Winding Magnetometer eddy current sensor, for example, is capable of detecting surface-breaking as well as subsurface discontinuities (Vladimir *et al.* 2001). The detection range of these sensors, however, is confined within the sensor's footprint area. To perform inspections over a large area, multiple sensing elements in parallel are needed. Wiring these sensors increases the size and weight of the cable and thus limits the maximum number of sensors that can be implemented. Wireless sensors are good candidates for densely distributed sensor networks (Hakozaki *et al.* 2001, Liu and Yuan 2008, Lynch 2005, Nagayama *et al.* 2009). In order to embed wireless sensors in sensing skins, however, the size of existing wireless sensor nodes have to be reduced substantially. In this regard, RFID based sensors nodes have advantages because of their small footprint (Morita and Kazuya 2006). RFID sensors consists of conductive strip-based crack sensors or conventional strain gauge sensors interfaced to a data acquisition and processing computer on-board the sensor. The digitized sensor data is then used to modulate the Radar Cross Section (RCS) of a compact antenna. The RFID reader demodulates the digital sensor measurement by detecting changes in the antenna RCS of the sensor. This type of sensor requires energy harvesting or an energy source on-board the sensor in order to power up the data acquisition and processing circuitry. For both conventional and RFID-based wireless sensor nodes, the need for power supply for the wireless sensors nodes needs to be addressed in order to be applicable for engineering sensor skins.

This paper presents a wireless antenna sensor that can be remotely interrogated without needing a local power source. In our previous publication (Mohammad and Huang 2010), the antenna sensor was interrogated by connecting a coax cable to the antenna and measuring the S_{11} parameter of the antenna sensor directly. A wireless interrogation technique that can interrogate the antenna sensor from a distance of 1.3 meter was also demonstrated on a bench-top (Deshmukh and Huang 2010). In this paper, the antenna sensor and the associated impedance-switching circuit were implemented on a fatigue specimen and subjected to fatigue cycling. The resonant frequency of the antenna sensor at different crack lengths was measured wirelessly during fatigue testing. Since the sensor can operate without any external wiring, it is straightforward to multiplex the sensors into a large sensor network. Other advantages of this sensor include direct damage detection, high spatial resolution, low profile, light weight, low fabrication cost, and conformability. All these characteristics render the wireless antenna sensor an ideal candidate as the sensing element for large area flexible sensor skins that can be used to monitor crack initiation and growth in engineering structures. This paper presents the experiment work that characterized the antenna sensor's performance for crack detection and monitoring. Remote interrogation of the antenna sensor using a microwave radar system is also discussed.

2. Principle of operation

The antenna sensor, as shown in Fig. 1(a), comprises of a dielectric substrate placed between a rectangular metallic patch and a ground plane. The metallic patch and the ground plane form an electromagnetic resonant cavity that can resonate at two fundamental modes. The radiation mode with its current flowing along the length dimension of the patch is termed TM_{01} mode while the one with the current flowing along the width direction of the patch is termed TM_{10} mode. The resonant
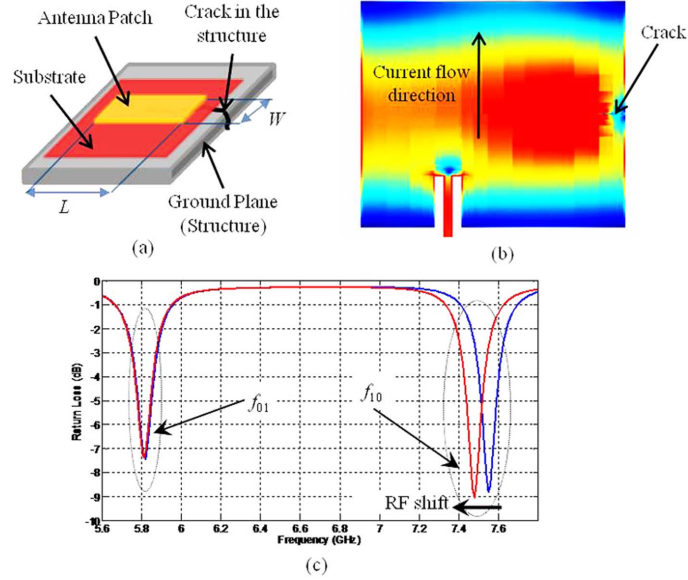
Fig. 1 Principle of antenna sensor: (a) patch antenna configuration, (b) effect of crack in ground plane on the current flow and (c) effect of crack on S_{11} parameters of patch antenna

frequencies corresponding to these two fundamental modes are then denoted as f_{01} and f_{10} frequency, respectively.

2.1 Principle of operation - crack detection

According to the transmission line model of the patch antenna, the resonant frequency of an antenna sensor without a crack in the ground plane is related to the electric length L_e as (Bhartia *et al.* 1991).

$$f_{res} = \frac{c}{2\sqrt{\varepsilon_{re}}} \frac{1}{L_e + 2\Delta L_{oc}} \tag{1}$$

where c is the speed of light in vacuum and ε_{re} is the effective dielectric constant of the substrate. ΔL_{oc}, the line extension, is an extension of effective patch dimension due to the fringe fields near the edge of the patch, which can be calculated from the patch and substrate dimensions and the substrate dielectric constant (Bhartia *et al.* 1991). Because of its thin substrate, ΔL_{oc} is very small for the antenna sensor and can be neglected. L_e, the electrical length of the patch, is defined as the effective dimension of the patch along the direction of the radiation mode. If there is no crack in the ground plane, L_e is the corresponding geometric dimension of the patch. For a ground plane with a crack, however, there is no analytical formula for calculating L_e. The effect of the crack on L_e and the antenna resonant frequency has to be simulated numerically. As shown in the numerically simulated current plot shown in Fig. 1(b), a crack perpendicular to the width of the antenna patch partially cuts off the current flow of the TM_{10} mode, forcing the current to flow around the crack. As a result, the average electric length of the TM_{10} current flow is increased due to the crack presence, which reduces the f_{10} resonant frequency. The magnitude of decrease in the resonant frequency is directly related to the length of the

crack under the antenna patch. Since the current flow along the length direction is not affected by the crack, the f_{01} resonant frequency remains the same. The effect of the crack on these two resonant frequencies can be illustrated using the S_{11} curve of the antenna sensor shown in Fig. 1(c). In contrast, a crack perpendicular to the length of the patch reduces the f_{01} resonant frequency but does not have any effect on the f_{10} frequency.

2.2 Principle of operation - wireless interrogation

Wireless interrogation of the antenna sensor can be achieved based on the principle of antenna backscattering. When a wideband interrogation signal is broadcasted to an antenna sensor, the antenna sensor will receive the signals whose frequency matches with the antenna's resonant frequency. If the antenna sensor is not terminated with a perfectly-matched load, the received signal will be reflected at the antenna termination and re-radiated by the antenna sensor. This re-radiated signal is called the antenna mode backscattering, which has the same frequency as the resonant frequency of the antenna sensor. Therefore, by performing spectrum analysis of the antenna mode backscattering, the resonant frequency of the antenna sensor can be determined. On the other hand, the structures surrounding the antenna reflect the interrogation signal indiscriminately, creating structural mode backscattering. In general, the structural mode backscattering is several orders higher in power than the antenna mode backscattering. As a result, the spectrum of the backscattered signal is dominated by the structural mode backscattering and the antenna frequency cannot be determined from this spectrum without separating the antenna mode backscattering from the structural mode back scattering. To isolate the antenna mode from the structure mode, impedance-switching can be implemented to obtain a normalized antenna mode backscattering, as shown in Fig. 2. A microwave switch that changes the antenna termination between open and short to the ground can be implemented at the end of the antenna feed line. By switching the two termination states, the antenna mode backscattering experiences a 180 degree phase difference while the structural mode remains the same. Subtracting the backscattered signal at these two states, therefore, doubles the antenna mode backscattering and cancels the structural mode backscattering. Based on this impedance-switching normalization scheme, we have demonstrated that the unpowered antenna sensor can be wirelessly interrogated from a distance of 1.3 meters away. The antenna sensor frequencies measured by the wireless means matched very well with the simulated resonant frequencies. More detailed description on the implementation and validation of the wireless interrogation scheme can be found in Deshmukh and Huang (2010).
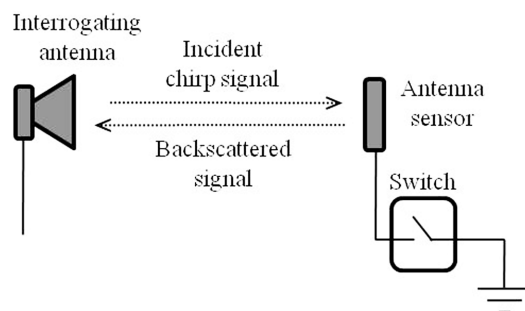

Fig. 2 Wireless interrogation based on impedance switching and backscattering

3. Specimen and antenna sensor fabrication

The antenna sensors were fabricated on pre-cracked compact tension (CT) specimens and were subjected to cyclic fatigue loading to evaluate the effect of crack growth on the antenna resonant frequency. The CT specimen was designed and machined according to ASTM standard E647-00. The as-machined CT specimen was first sanded to achieve a flat surface, followed by polishing using 400-grit sand paper to roughen the surface. A rectangular dielectric substrate (Kapton 300FN929, 70 μm in thickness, 50 mm in length, and 38 mm in width) was bonded to the specimen using glue that is certified for fatigue testing (Vishay M-bond AE-15). To ensure a good bonding, the bottom surface of the Kapton was slightly sanded. A 36 μm thick copper strip (3 M 1181, 15 mm long and 12.75 mm wide) was then bonded on top of the Kapton film using super glue. The dimensions of the patch are shown in Fig. 3(a). The size of the antenna patch was selected for the convenience of manual fabrication, which limits the antenna sensor frequency to be below 10 GHz. Another consideration is that the resonant frequency of the antenna sensor should be above 5 GHz so that the ambient interference can be minimized. Once the f_{10} and f_{01} frequencies are selected, the dimensions of the antenna patch can be determined based on Eq. (1) using the selected substrate dielectric constant and thickness (Mohammad and Huang 2010).

A light-activated remote microwave switch was implemented on the CT specimen using a microstrip feed line, a pHEMT (ATF 36077), a 560 KΩ resistor, and a photocell (Clare, CPC 1832). The narrow microstrip feed line was made from the copper strip and placed at the inset point of the copper sheet to achieve a 50 Ω impedance match. The feed line and the antenna patch were conductively joined using conductive epoxy. The photocell produces a voltage when illuminated by light, thus switching the pHEMT from short-to-the-ground to open-to-the-ground. The resistor is used to regulate the voltage output of the photocell. The fabrication procedure of the microwave switch is as follows. First, the pHEMT was bonded to the Kapton by placing its drain terminal next to the end of the antenna feed line. The source terminal of the pHEMT was connected to the specimen through a small cut-out, which serves as the electric ground. The resistor and the photocell were placed near the pHEMT gate terminal and bonded to the Kapton using super glue. Conductive epoxy was applied to connect the antenna feed line, the electronic components, and the specimen. Following the fabrication, the CT specimen was baked at 60°C for 4 hours to cure the conductive epoxy. The fabricated specimen/sensor assembly is shown in Fig. 3(b). The position of the
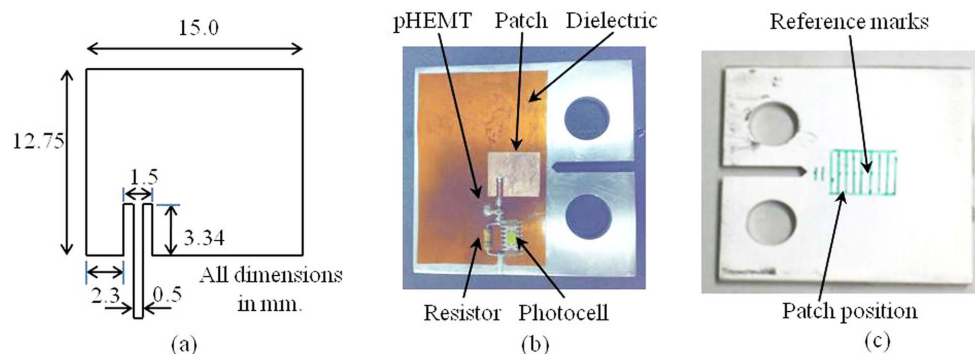

Fig. 3 Fatigue specimen: (a) antenna design, (b) wireless antenna sensor and (c) reference marks on the back side of the specimen

antenna sensor was marked on the opposite side of the CT specimen and reference marks with a separation of 2 mm were drawn on the specimen so that the crack growth can be visually monitored using a digital camera. A picture of the CT specimen showing the antenna patch position and the reference marks is given in Fig. 3(c).

4. Numerical simulation model

To understand the effect of a ground plane crack on the resonant frequency of the antenna sensor, the antenna sensor with a cracked ground plane was simulated using a commercial EM simulation tool, Sonnet Pro. The 3D numerical model, as shown in Fig. 4(a), was made up of three layers; the first layer is a lossless metal patch, the second layer is the dielectric substrate (Kapton, $\varepsilon_r = 2.5$, thickness = 50 μm), and the last layer is a lossless metal layer serving as the ground plane. The simulation model assumes the patch layer and the ground plane to have zero thickness so that the computation time can be drastically reduced. The dimensions of the patch, given in Fig. 4(b), were designed to resonate at 7.4 GHz and 6.3 GHz. The position of the antenna inset feed was optimized to match the feed impedance to 50 Ω along the width direction to reduce the return loss. Based on the theoretical crack opening, the ground plane crack was modeled as a 10 μm wide rectangular slot in the ground plane. Since the fringing fields from the patch antenna cavity do not exceed 0.1 mm from the patch edge, the cracks in the ground plane beyond 0.1 mm have little effect on the patch antenna resonant frequency. Thus, the crack was initiated at 0.1 mm from the patch edge, perpendicular to the width dimension. In addition, to lessen the computation burden, the ground plane dimensions were selected to cover the fringe field of the antenna only, which is much smaller than the actual ground plane of the antenna sensor. The simulation cell dimensions dictate the spatial resolution of the simulation model. Smaller simulation cell sizes result in more accurate modeling of the structure but significantly increase the computation time required. In this simulation, the simulation cell size was set to be 0.1 mm by 0.01 mm. The parallel subsections near the feed line were eliminated and an adaptive frequency sweep (ABS) was used to reduce the simulation time. The simulator was configured to analyze the S_{11} parameter from 4.0 GHz to 7.8 GHz while the crack length parameter was swept from 0 mm to 7.0 mm.
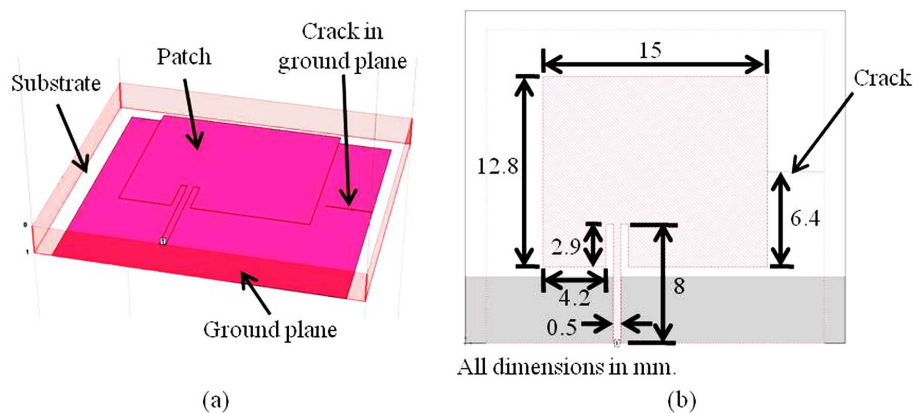

Fig. 4 Numerical simulation model of antenna sensor: (a) 3D model and (b) dimensions

5. Experimental procedures

Two experiments were designed and carried out to characterize the antenna sensor and the remote interrogation system. The first one, fatigue testing of the antenna sensor on CT specimens was aimed to quantify the antenna sensor's sensitivity to fatigue crack growth. The second experiment evaluates the response of the antenna sensor when the interrogating horn antenna and the antenna sensor were orientated at an angle.

5.1 Fatigue experiment

Remote interrogation of the antenna sensor during fatigue testing is shown in Fig. 5(a). The CT specimen was mounted on a mechanical testing frame using clevises and pins. A CCD camera was placed facing the opposite side of the antenna sensor. Digital images of the cracked region of the specimen were acquired using a LabView program into a computer and displayed on a monitor to track the crack propagation. The antenna sensor was interrogated wirelessly using a monostatic radar system shown in Fig. 5(b). A horn antenna, placed in front of the antenna sensor at a distance of 36 inches, was connected to port 1 of a Vector Network Analyzer (VNA), which was configured to sweep from 5 GHz to 9 GHz in 8000 points. The VNA was calibrated with its reference plane at the end of the cable and the power output of the VNA was set to 25 dBm. A light source was used to illuminate the photocell and thus activate the impedance switching. The brightness of the light source was adjusted to maintain a -1.5 volt gate-to-source voltage for the pHEMT. The light source was triggered using the computer's parallel port through a relay (OEG model OUAZ-SS-105D). A Microsoft Excel program was developed to control the light source and the VNA, which initiates the VNA at the beginning of the test, triggers the VNA to collect data at different antenna termination states, receives the data and stores them in the hard drive of the computer. Each measurement consists of two steps. The spectrum of the backscattered signal was first measured when the light source was turned OFF. At this state, the pHEMT is in saturation mode and the antenna sensor is shorted to the
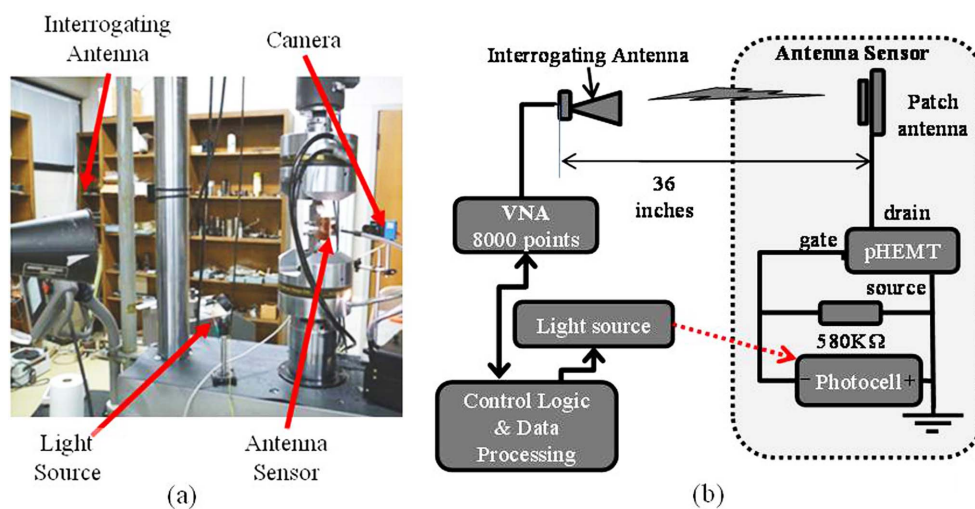

Fig. 5 Experimental setup: (a) actual setup and (b) schematic for wireless interrogation

ground. The light source was then turned ON to bias the pHEMT into the cut-off mode and thus terminate the antenna sensor in open circuit. The VNA was again triggered to collect the spectrum of the backscattered signal. The measured spectra were downloaded from the VNA to a computer for data processing.

The CT specimen was first subjected to a fatigue loading (5 Hz loading frequency, $P_{max} = 600$ lb, and $R = 0.5$) using a closed loop servo-hydraulic MTS machine to initiate pre-cracking and to propagate the crack under the antenna patch. Whenever the crack reached a reference mark, the fatigue cycling was paused at a static load of 300 lbs. The resonant frequency of the antenna sensor was then measured by triggering a measurement sequence using the Microsoft Excel program. Ten measurements were recorded for each crack length and the average resonant frequency was calculated. After completing the measurement process, the fatigue cycling was resumed until the crack reached the next reference mark. The fatigue test was continued until cracking of the antenna patch was observed due to large crack opening.

5.2 Evaluating angular response of the antenna sensor

To characterize the effect of the interrogation antenna orientation on the response of the antenna sensor, an experimental set-up allowing the antenna sensor to be precisely rotated about three directions, i.e., the elevation, azimuth, and polarization direction, was implemented (see Fig. 6). The polarization axis of the antenna sensor was parallel to the axis of the horn antenna, the elevation axis was parallel to the antenna length direction, and the azimuth axis was parallel to the antenna width direction. The antenna sensor was placed at a distance of 53 inches from the interrogating horn antenna. A laser pointer was placed next to the horn antenna, pointing at the photocell on the antenna sensor. By connecting the horizontal feed of the horn antenna to the VNA, the polarization of the horn antenna radiation was aligned along the elevation axis, i.e., the length direction, of the antenna patch. The antenna resonant frequencies were measured at an elevation angle of -45, -30, -10, 0, and 10 degrees, an azimuth angle of -45, -30, 0, 10, 30, and 45 degrees, and a polarization angle of 0, 10, 30, 45, 60, and 90 degrees.

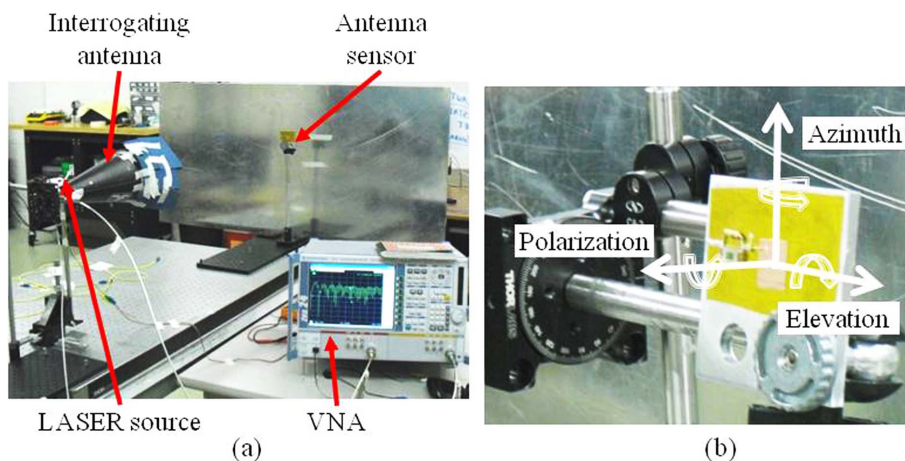Fig. 6 Experiment setup for angular response measurement of the sensor: (a) actual setup and (b) rotation directions

6. Results and analysis

6.1 Fatigue test results

As the crack propagated underneath the antenna patch, shifting of the f_{10} frequency of the antenna sensor to lower values was observed, as shown in Fig. 7. The rightmost curve (blue color) in Fig. 7(a) represents the f_{10} frequency of the antenna sensor when the crack was at the left edge of the antenna patch, i.e., there was no overlap between the crack and the antenna patch. Each subsequent shift of the curve to the left corresponds to a crack propagation of 1 mm. The signal strength of the backscattered antenna mode signal reduced with the crack growth. As a result, the Signal to Noise Ratio (SNR), defined as the ratio between the amplitude of the antenna mode and the average amplitude of the noise floor, also reduced. Cracking of the antenna patch right above the crack was observed as the crack opening increased with the crack growth. This might have contributed to the reduction of SNR. Defining the left edge of the antenna patch as the origin of the crack tip location and normalizing the frequencies at different crack lengths with the antenna frequency at crack location 0, the shift of the f_{10} frequencies obtained using three different methods, i.e., wireless interrogation, numerical simulation, and wired measurement, are compared in Fig. 7(b). The f_{10}
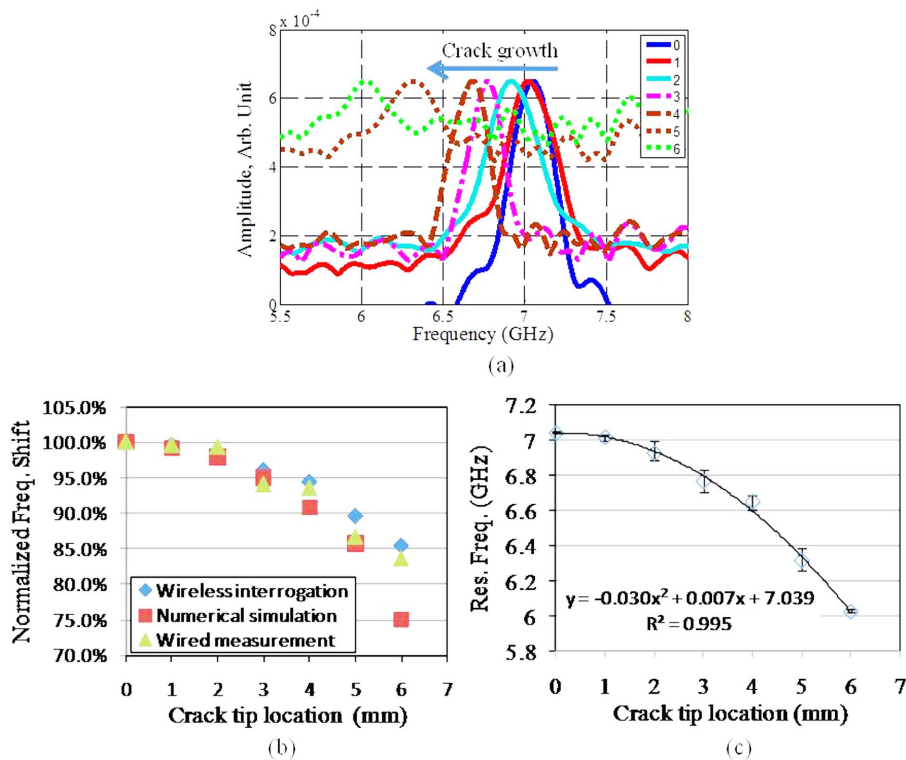

Fig. 7 Effect of crack on the f_{10} frequency of the antenna sensor under a 300 lbs load: (a) shift of the antenna mode spectrum with crack growth, (b) comparison of normalized f_{10} frequency shifts obtained by wireless interrogation, numerical simulation, and wired measurements and (c) shift of the f_{10} frequency with crack growth (the average and error bar at location 1mm and 6 mm were calculated from 4 and 5 measurements, respectively. The other data points were calculated from 10 measurements)

frequency did not shift linearly with the crack growth. This is different from what was reported in Mohammad and Huang (2010) because the frequencies used in that paper were actually the frequencies of TM_{011} mode instead of the TM_{010} mode. By properly placing the inset feed, the return loss of the TM_{010} mode can be minimized and the TM_{011} mode can be suppressed. It worth noting that the simulation model was simplified to reduce computation time, e.g., the thickness of the ground plane was assumed to be zero. A full scare three-dimensional simulation of the antenna sensor may result in better agreements but the required computation time is prohibiting. Even though the relationship between the frequency shift and the crack growth is not linear, the crack length can be determined from the frequency shift as long as the relationship is calibrated. As shown in Fig. 7(c), the shift of the wirelessly measured f_{10} frequencies with the crack length fit a second order polynomial very well. From location 0 to location 1, 1 mm of crack growth shifted the f_{10} frequency by 24.85 MHz. As the crack grew under the antenna patch, the crack sensitivity increased steadily. From location 5 to location 6, 1 mm of crack growth resulted in a frequency shift of 292.5 MHz. Judging from the error bars presented in Fig. 7(c), we are confident that sub-millimeter crack growth can be detected using the antenna sensor. In this paper, only a crack that is parallel to the length direction of the antenna patch was evaluated. A crack that is parallel to the width direction of the antenna patch should have similar effects on the f_{01} frequency.

We used a frequency domain measurement instrument (VNA) for the wireless interrogation of the antenna sensor. A Time Domain Reflectometer (TDR) based digital storage oscilloscope having a noise floor less than -65 dBm can be used for this interrogation technique as well. In this case, the
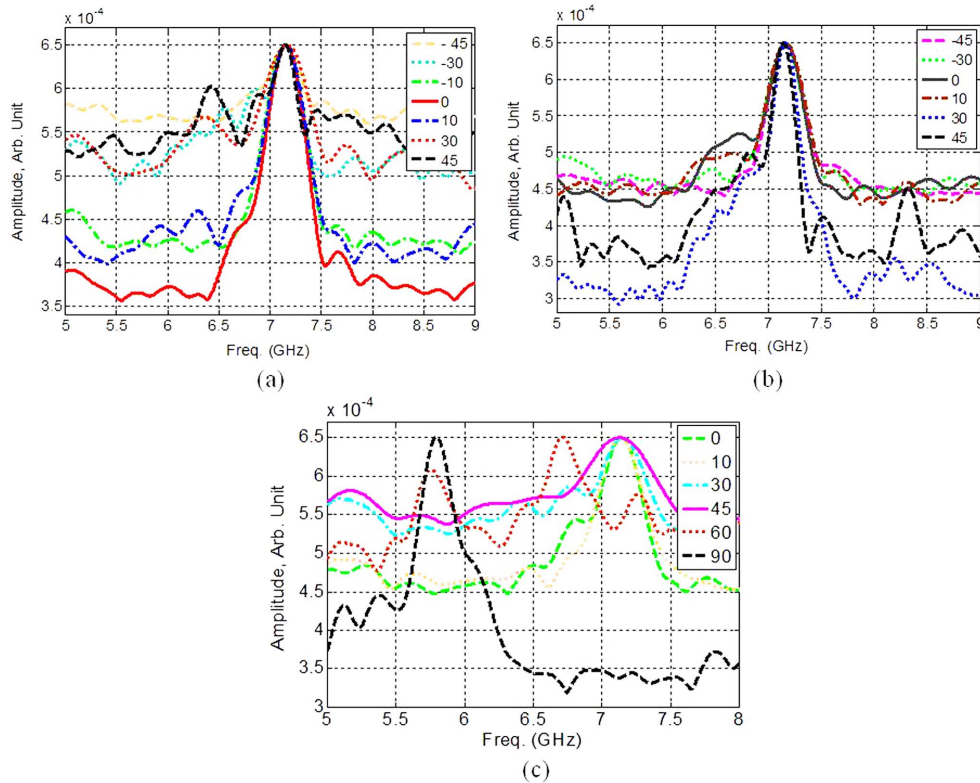

Fig. 8 Angular response of the antenna sensor: (a) elevation direction, (b) azimuth direction and (c) polarization

control logic and the data processing tasks can be integrated into the oscilloscope instrument, thus reducing the cost and complexity of the detection equipment.

6.2 Angular response of the antenna sensor

The spectra of the antenna mode backscattering for various elevation angles are shown in Fig. 8(a). The SNR was the highest when the antenna sensor was oriented at zero degrees. As the angle of rotation increased, the resonance peak remained at the same frequency while the SNR reduced. This indicates that the measured antenna frequencies are not very sensitive to the angular alignment. The f_{10} frequency of the antenna sensor can be reliably measured as long as the antenna sensor and the horn antenna were aligned within 30 degrees. The spectra of the antenna mode backscattering at different azimuth angles are shown in Fig. 8(b). Again the frequency peak locations were not sensitive to the angle changes but the SNR is. The maximum SNR was achieved at an azimuth angle of 30 degrees instead of zero degree. This might be contributed by the feed line not locating along the center line of the patch, which could produce a radiation pattern that is not symmetric about the zero degree azimuth angle (Makarov 2002). Rotating the antenna sensor along the polarization direction essentially changes the orientation of the antenna patch relative to the polarization of the horn antenna radiation. At zero degrees, the width direction of the antenna patch was parallel to the polarization of the horn antenna radiation. Therefore, only the f_{10} frequency was observed (see Fig. 8(c)). For a polarization angle increase up to 45 degrees, the f_{10} frequency behaved similarly as when the elevation and azimuth angle was increased, i.e., the resonance frequency remained at the same frequency while the SNR decreased. At a polarization angle of 60 degrees, the f_{01} frequency started to emerge and the f_{10} frequency disappeared. At 90 degrees, the length direction of the antenna patch was aligned with the polarization of the electromagnetic field. As such, only the f_{01} frequency was visible. Even though the f_{10} frequency was insensitive to the polarization angles up to 45 degrees, the f_{01} frequency seems to be more sensitive to the polarization angle arrangement, e.g., at 60 degree polarization angle, the f_{01} frequency peak was not as distinguishable as the f_{10} frequency peak at 30 degree polarization angle. This might be explained by the radiation patterns. Due to the feed line configuration, the radiation pattern of these two radiation modes are different, as evidenced by the current plots shown in Fig. 9. Nevertheless, this experiment demonstrated that
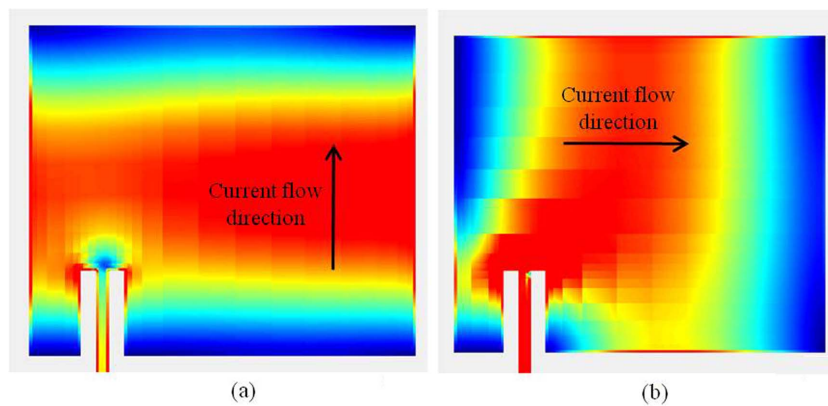

(a)   (b)

Fig. 9 Current plots of (a) TM_{10} and (b) TM_{01} radiation modes

the two fundamental resonant frequencies of the antenna sensor can be remotely interrogated using one rotating horn antenna or using a horn antenna with dual polarizations.

7. Conclusions

This paper presented an antenna sensor that can detect sub-millimeter crack growth and can be interrogated wirelessly without needing any local power supply. The antenna sensor has many unique features, including simple configuration, low profile, light weight, and conformal, *etc*. Fatigue testing of the antenna sensor bonded on CT specimens demonstrated that the antenna sensor is capable of sustain tens of thousands of fatigue cycles without losing its functionality. For long-term real-life applications, the antenna sensor can be coated with a microwave-transparent protective coating or enclosed in a radome to protect it from the environment. In addition, the crack pattern can be very complex in practical scenarios. We are currently working on multiplexing these antenna sensors to achieve a sensor skin that can detect multiple cracks with various orientations. The design and evaluation of such a sensor skin will be a subject of future publications.

Acknowledgements

References

Axelrod, F.B. and Hilz, M.J. (2003), "Inherited autonomic neuropathies", *Semin Neurol*., **23**(4), 381-90.
Bhartia, P., Rao, K. and Tomar, R. (1991), Millimeter-wave Microstrip and Printed Circuit Antennas, Artech House.
Carlson, J.A., English, J.M. and Coe, D.J. (2006), "A flexible, self-healing sensor skin", *Smart Mater. Struct*., **15**(5), N129-N135.
Chang, F.K. and Ihn, J.B. (2004), "Detection and monitoring of hidden fatigue crack growth using a built-in piezoelectric sensor/actuator network: I. Diagnostics", *Smart Mater. Struct*. **13**(3), 609-620.
Deshmukh, S. and Huang, H. (2010), "Wireless interrogation of antenna sensor", *Meas. Sci. Technol*., **21**, 035201.
Giurgiutiu, V. and Bao, J. (2002), "Embedded-ultrasonics structural radar for in situ structural health monitoring of thin-wall structures", *Struct. Health Monit*. **3**, 121-140.
Hakozaki, M., Hatori, A. and Shinoda, H. (2001), "A sensitive skin using wireless tactile sensing elements", *Proceedings of the Technical Digest of the 18th sensor symposium*, 147-150.
Jang, J., Frank, J.L., Patrick, C.Y. and Sohn, H. (2006), "Development of self-contained sensor skin for highway bridge monitoring", *Proceedings of the SPIE*, 6174 II, 617441.
Liu, L. and Yuan, F.G. (2008), "Wireless sensors with dual-controller architecture for active diagnosis in structural health monitoring", *Smart Mater. Struct*., **17**(2), 025026.
Loh, K.J., Hou, T.C, Lynch, J.P. and Kotov, N.A. (2009), "Carbon nanotube sensing skins for spatial strain and impact damage identification", *J. Nondestruct. Eval*., **28**(1), 9-25.
Lynch, J. (2005), "Design of a wireless active sensing unit for localized structural health monitoring", *Struct. Health*

Monit., **12**(3-4), 405-423.

Makarov, S.N. (2002), *Antenna and EM Modeling with MATLAB*, John Wiley and Sons, Inc, New York.

Mohammad, I. and Huang, H. (2010), "Monitoring fatigue crack growth and opening using antenna sensors", *Smart Mater. Struct.*, **19**(5), 055023.

Morita, K., Kazuya, N. (2006), "Crack detection sensor using RFID-tag and electrically conductive paint", *AIJ J. Technol. Design*, **24**, 73-76.

Nagayama, T., Spencer Jr., B.F. and Rice, J.A., (2009), "Autonomous decentralized structural health monitoring using smart sensors", *Struct. Health Monit.*, **16**(7-8), 842-859.

Shoureshi, R. and Shen, A. (2006), "Self-powered sensory nerve system for civil structures using hybrid forisome actuators", *Proceedings of the SPIE*, 6174, 617438.

Smith, J. (1989), *Senses and Sensibilities*, John Wiley & Sons.

Verpoorten, N., et al. (2006), "Novel frameshift and splice site mutations in the neurotrophic tyrosine kinase receptor type 1 gene (NTRK1) associated with hereditary sensory neuropathy type IV", *Neuromuscul. Disord.*, **16**(1), 19-25.

Woolf, C.J. and Ma, Q. (2007), "Nociceptors - noxious stimulus detectors", *Neuron.*, **55**(3), 353-64.

Zilberstein, V., Schlicker, D., Walrath, K., Weiss, V. and Goldfine, N. (2001), "MWM eddy current sensors for monitoring of crack initiation and growth during fatigue tests and in service", *Int. J. Fatigue*, **23**(1), S477-S485.

Zhang, B., Zhou, Z., Zhang, K., Yan, G. and Xu, Z. (2006), "Sensitive skin and the relative sensing system for real-time surface monitoring of crack in civil infrastructure", *J. Intel. Mat. Syst. Str.*, **17**(10), 907-917.